

EVDodgeNet: Deep Dynamic Obstacle Dodging with Event Cameras

Nitin J. Sanket¹, Chethan M. Parameshwara¹, Chahat Deep Singh¹, Ashwin V. Kuruttukulam¹,
Cornelia Fermüller¹, Davide Scaramuzza², Yiannis Aloimonos¹

Abstract—Dynamic obstacle avoidance on quadrotors requires low latency. A class of sensors that are particularly suitable for such scenarios are event cameras. In this paper, we present a deep learning – based solution for dodging multiple dynamic obstacles on a quadrotor with a single event camera and on-board computation. Our approach uses a series of shallow neural networks for estimating both the ego-motion and the motion of independently moving objects. The networks are trained in simulation and directly transfer to the real world without any fine-tuning or retraining. We successfully evaluate and demonstrate the proposed approach in many real-world experiments with obstacles of different shapes and sizes, achieving an overall success rate of 70% including objects of unknown shape and a low light testing scenario. To our knowledge, this is the first deep learning – based solution to the problem of dynamic obstacle avoidance using event cameras on a quadrotor. Finally, we also extend our work to the pursuit task by merely reversing the control policy, proving that our navigation stack can cater to different scenarios.

SUPPLEMENTARY MATERIAL

The accompanying video and supplementary material are available at <http://prg.cs.umd.edu/EVDodgeNet>.

I. INTRODUCTION AND PHILOSOPHY

The never-ending quest to understand and mimic ultra-efficient flying agents like bees, flies, and birds has fueled the human fascination to create autonomous, agile and ultra-efficient small aerial robots. These robots are not only utilitarian but are much safer to operate in static or dynamic environments and around other agents as compared to their larger counterparts. Need for creation of such small aerial robots has given rise to the development of numerous perception algorithms for low latency obstacle avoidance. Here, latency is defined as the time the robot takes to perceive, interpret and generate control commands [1].

Low latency static obstacle avoidance has been studied extensively in the last decade [2]. Recently, however, dynamic obstacle avoidance has gained popularity in the field of robotics due to the exponential growth of event cameras. These are bioinspired vision sensors that output per-pixel temporal intensity differences caused by relative motion with microsecond latency [3].

Event cameras have the potential to become the de-facto standard for visual motion estimation problems due to their inherent advantages of low latency, high temporal resolution, and high dynamic range [4]. These advantages make event cameras tailor made for dynamic obstacle avoidance.

In this paper, we present a framework to dodge multiple unknown dynamic obstacles on a quadrotor with event cameras using deep learning. Although dynamic obstacle detection using traditional cameras and deep learning

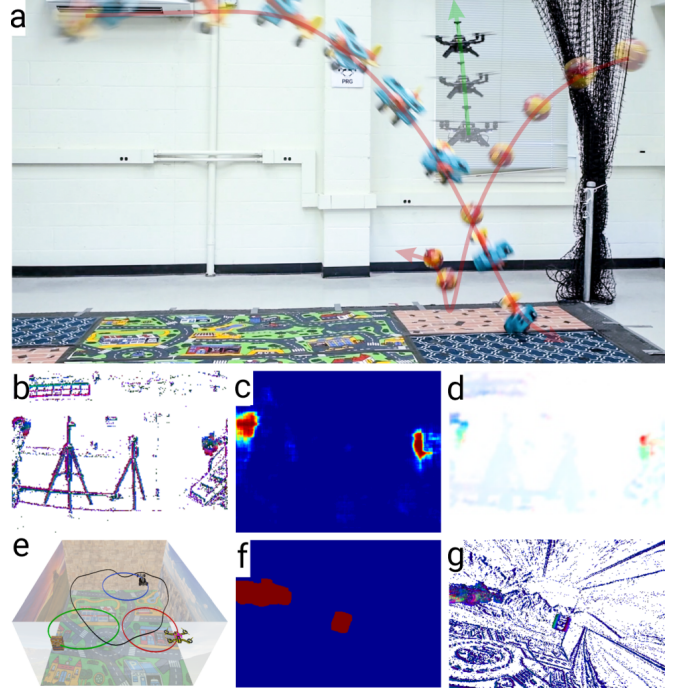


Fig. 1. (a) A real quadrotor running *EVDodgeNet* to dodge two obstacles thrown at it simultaneously. (b) Raw event frame as seen from the front event camera. (c) Segmentation output. (d) Segmentation flow output which includes both segmentation and optical flow. (e) Simulation environment where *EVDodgeNet* was trained. (f) Segmentation ground truth. (g) Simulated front facing event frame. All the images in this paper are best viewed in color.

has been extensively studied in the computer vision community under the umbrellas of object segmentation and detection, they are either of high latency, computationally expensive (not enough to be used on to be used on micro/nano-quadrotors) and/or do not generalize to novel objects without retraining or fine-tuning.

Our work is closely related to [1] with the key difference being that our approach uses deep learning and generalizes to unknown real objects after being trained only on simulation.

A. Problem Formulation and Contributions

A quadrotor moves in a static scene with multiple Independently Moving dynamic Objects/obstacles (IMOs). The quadrotor is equipped with a front facing event camera, a downfacing lower resolution event camera coupled with sonar, for altitude measurements, and an IMU.

The problem we address is as follows: *Can we present an AI framework for the task of dodging/evading/avoiding these dynamic obstacles without any prior knowledge, using only on-board sensing and computation?*

We present various flavors of the dodging problem, such as hovering quadrotor dodging unknown obstacles, slow-moving quadrotor dodging unknown shaped obstacles given a bound on size, hovering and slow moving quadrotor

Nitin J. Sanket and Chethan M. Parameshwara contributed equally to this work. (Corresponding author: Nitin J. Sanket.)

¹Perception and Robotics Group, University of Maryland Institute for Advanced Computer Studies, University of Maryland, College Park.

²Robotics and Perception Group, Dep. of Informatics, University of Zurich, and Dep. of Neuroinformatics, University of Zurich and ETH Zurich.

dodging known objects (particularly targeted to spherical objects of known radii).

We also broaden the horizon of our approach by demonstrating pursuit/intercept of a known object using the same deep-learning framework. This showcases that our proposed framework can be used in a general navigation stack on a quadrotor and can be re-purposed for various related tasks.

A summary of our contributions is given below (Fig. 1):

- We propose and implement a network (called EVDeBlurNet) that *deblurs* event frames, such that learning algorithms trained on simulated data can generalize to real scenes without retraining or fine-tuning.
- We design and implement a network (called EVSegFlowNet) that performs both segmentation and optical flow of IMOs to obtain both segmentation and optical flow in a single network.
- We propose a control policy based on estimated motion of multiple IMOs under various scenarios.
- We evaluate and demonstrate the proposed approach on a real quadrotor with onboard perception and computation.

B. Related Work

We subdivide the related work into three parts, i.e., ego-motion estimation, independent motion segmentation, and obstacle avoidance.

1) *Independent Motion Detection and Ego-motion Estimation – Two sides of the same coin:* Information from complementary sensors, such as standard cameras and Inertial Measurement Units (IMUs), has given rise to the field of Visual Inertial Odometry (VIO) [5]–[7]. Low latency VIO algorithms based on event cameras have been presented in [4], [8], which use classical feature tracking inspired methods to estimate ego-motion. Other works, instead, try to add semantic information to enhance the quality of odometry by adding strong priors about the scene [9], [10]. Most works in the literature focus on ego-motion estimation in static scenes which are seldom encountered in the real world. To account for moving objects, these algorithms implement a set of outlier rejection schemes to detect IMOs. We would like to point out that by carefully modelling these “outliers” one can estimate both ego-motion and IMO motion [11].

2) *Image stabilization as a key to independent motion segmentation:* Keen readers might have contrived that by performing the process of image stabilization IMOs would “stand-out”. Indeed, this was the approach most robust algorithms used in the last two decades. A similar concept was adapted in some recent works on event-based cameras for detecting IMOs [12]–[14]. Recently a deep learning based approach was presented for IMO detection using a structure from motion inspired approach [15].

3) *Obstacle avoidance on aerial robots:* The works presented in the above two subsections have aided the advancement of obstacle avoidance on aerial robots. [16], [17] presented approaches for high speed static obstacle avoidance by estimating depth maps and visual servoing using a monocular imaging camera respectively. [18] provides a detailed collation of the prior work on static obstacle avoidance using stereo cameras. A hardware and software architecture was proposed in [19], [20] for high speed quadrotor navigation by mapping the cluttered

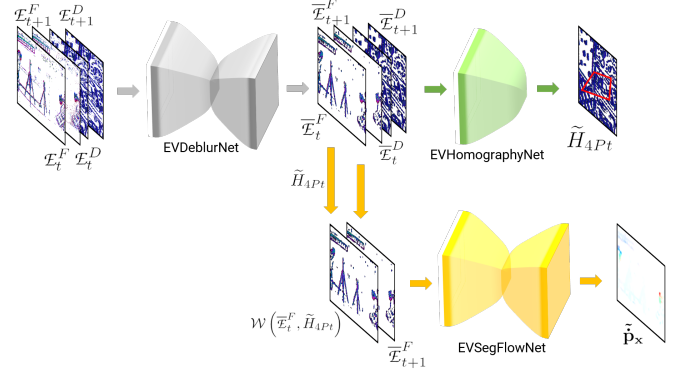


Fig. 2. Overview of the proposed neural network based navigation stack for the purpose of dodging.

environment using a lidar. Using event cameras for high speed dodging is not new and the first work was presented in [21] where an approach was presented to avoid a dynamic spherical obstacle using stereo event cameras. Very recently, [1] presented a detailed analysis of perception latency for dodging a dynamic obstacle.

C. Organization of the paper

The paper is structured into perception and control modules. The perception module (Refer to Fig. 2) is further divided into three segments.

1. The input to the perception system are event frames (Sec. II-B). Such a projection of event data to generate *event frames* suffers from misalignment [22] unless motion compensation is performed. We call this misalignment or loss of contrast/sharpness as *blur* due to its visual resemblance to classical image motion blur. To perform motion compensation and denoising, we present a neural network called *EVDeBlurNet* in Sec. II-B.

2. Sec. II-C presents how ego-motion is obtained using *EVHomographyNet*.

3. Sec. II-D describes how segmentation and optical flow of IMOs are obtained using the novel *EVSegFlowNet*.

Sec. III presents the control scheme for dodging given the outputs from the perception module. We also bring the generality of our perception stack into limelight in Sec. III-D by adapting our approach to the problem of pursuit. Sec. IV illustrates the experimental setup and provides error analyses of the approaches presented along with detailed ablation studies. We finally conclude the paper in Sec. V with parting thoughts on future work.

II. DEEP LEARNING BASED NAVIGATION STACK FOR DODGING DYNAMIC OBSTACLES

An overview of our proposed approach is illustrated in Fig. 2.

A. Definitions Of Coordinate Frames Used

The letters I, E^F, E^D, S and W denote coordinate frames on the Inertial Measurement Unit (IMU), front facing event camera, down facing event camera, down facing sonar and the world respectively (Fig. 3). All the sensors are assumed to be rigidly attached with the intrinsic and extrinsic calibration between them known. A pinhole camera model is used for the formation of the image. The world point \mathbf{X} gets projected onto the image plane point \mathbf{x} . Unless otherwise stated, the points on the image plane are used after rectification.

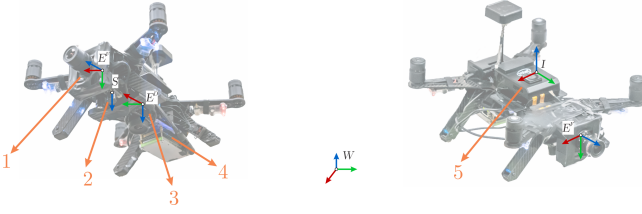


Fig. 3. Representation of coordinate frames on the hardware platform used. (1) Front facing DAVIS 240C, (2) down facing sonar on PX4Flow, (3) down facing DAVIS 240B, (4) NVIDIA TX2 CPU+GPU, (5) Intel® Aero Compute board.

B. EVDeBlurNet

The event frame \mathcal{E} consists of three channels. The first and second channels contain the per-pixel average count of positive and negative events. The third channel contains the per-pixel average time (refer to Section S.I for a mathematical formulation). Though event representation offers many advantages regarding computational complexity and providing tight time bounds on operation, there is a hitch. Event frames can be “blurry” (projection of misaligned events) based on a combination of the integration time δt (observe in Fig. 9 how sharpness of the image decreases as integration time δt increases), apparent scene movement on the image plane (which depends on the amount of camera movement and depth of the scene) and scene contrast (contrast of the latent image pixels). Here, we define blur on the event frame \mathcal{E} as the event triggers from the same point on the world not being aligned on the image plane in a small integration time δt due to the way events are triggered on the sensor and accumulated in our formulation. An event is triggered when the relative contrast (on the latent image I) exceeds a threshold τ and is mathematically modelled as

$$\|\log(I)\|_1 \approx \|\langle \nabla_{\mathbf{x}} \log(I), \dot{\mathbf{x}} \Delta t \rangle\|_1 \geq \tau \quad (1)$$

Here, $\nabla_{\mathbf{x}}$ is the spatial gradient, $\dot{\mathbf{x}}$ is the motion field on the image and Δt is the time since the previous event at the same location. The above equation elucidates how the latent image contrast, motion and depth are coupled to event frames. Note that, $\dot{\mathbf{x}}$ depends on the 3D camera motion and the scene depth. We refer the reader to [23] for more details.

This “blurriness” of the event frame can adversely affect the performance of algorithms built on them. To alleviate this problem, we need to deblur the event images. This is fairly easy if we directly use the spatio-temporal event cloud and follow the approach described in [22]. Essentially the problem deals with finding point trajectories along the spatio-temporal point cloud to maximize a heuristically chosen contrast function. Mathematically, we want to solve the following problem.

$$\arg\max_{\theta} \mathcal{C}(\mathcal{W}(\mathcal{E}, \theta)) \quad (2)$$

where \mathcal{C} is a heuristic contrast function and θ are the parameters of point trajectories in the spatio-temporal point cloud according to which the events are warped and $\mathcal{W}(\mathcal{E}, \theta)$ represents the event image formed by the warped events. In our scenario, we want to model the deblurring problem in 2D, i.e., working on \mathcal{E} directly without the use of a spatio-temporal point cloud so that the problem can be solved efficiently using a 2D Convolutional Neural Network (CNN). Such a deblurring problem using a single image has been studied extensively for traditional cameras for rectifying motion blurred photos. Our modified problem in 2D can be

formulated as:

$$\arg\max_{\mathcal{K}} \mathcal{C}(\mathcal{K} \otimes \mathcal{E}) \quad (3)$$

Here \mathcal{K} is the heterogeneous deblur kernel and \otimes is the convolution operator. However, estimating \mathcal{K} directly is not constrained enough to be learned in an unsupervised manner. Instead, we formulate the deblurring problem inspired by Total Variation (TV) denoising to give us the final optimization problem as follows:

$$\arg\max_{\bar{\mathcal{E}}} \mathcal{C}(\bar{\mathcal{E}}) + \lambda \arg\min_{\bar{\mathcal{E}}} \mathcal{D}(\mathcal{E}, \bar{\mathcal{E}}) \quad (4)$$

where $\bar{\mathcal{E}}$ represents the deblurred event frame, λ is a regularization penalty and \mathcal{D} represents a distance function to measure similarity between two event frames. Note that directly solving $\arg\max_{\bar{\mathcal{E}}} \mathcal{C}(\bar{\mathcal{E}})$ yields trivial solutions of high frequency noise.

To learn the function using a neural network we convert the $\arg\max$ operator into an $\arg\min$ operator as follows:

$$\arg\min_{\bar{\mathcal{E}}} -\mathcal{C}(-\bar{\mathcal{E}}) + \lambda \mathcal{D}(\mathcal{E}, \bar{\mathcal{E}}) \quad (5)$$

Intuitively, the higher the value of the contrast, the lower the value of the loss function, but going away too far from the input will penalize the loss function striking a balance between high contrast and similarity to the input image. We call our CNN which generates the deblurred event images *EVDeBlurNet*. It takes as input \mathcal{E} and outputs deblurred $\bar{\mathcal{E}}$. The network architecture is a simple Encoder Decoder with four convolutional and four deconvolutional layers with batch normalization (Supplementary material Section S.III). Another benefit which can be intuited due to the encoder decoder’s lossy reconstruction is that it removes stray events which are generally noise and retains only events corresponding to contours of real-world scene objects or strong edges and this greatly increases the signal to noise ratio.

C. EVHomographyNet

A simple and computationally inexpensive way to obtain odometry on a quadrotor is to use a downfacing camera looking at a planar surface. This approximation coupled with data from an IMU and a distance sensor enables high speed “cheap” odometry for navigation. Recently, deep learning approaches have shown more robust homography estimation in traditional images [24], [25]. Inspired by this, we propose the first deep learning based solution to the problem of homography estimation using event cameras which can be run on an embedded computer at reasonably high speeds and good accuracy. Also, the added benefit of using a deep network for homography is that the tradeoff between speed and accuracy could be altered easily (by changing number of parameters). Let us mathematically formulate our problem statement. Let \mathcal{E}_t and \mathcal{E}_{t+1} be the event frames captured at times t and $t+1$, respectively, and $\delta t \ll \Delta t$ where Δt is the time difference between the start times of event frame accumulation. In the scenario presented before, the transformation between the two events frames is a homography. This can be written as $\mathbf{x}_{t+1} = \mathbf{H}_t^{t+1} \mathbf{x}_t$, where $\mathbf{x}_{t+1}, \mathbf{x}_t$ represent the homogeneous point correspondences in the two event frames and \mathbf{H}_t^{t+1} is the resulting non-singular 3×3 homography matrix between the two frames. We adapt the previous works on deep learning

based homography estimation [24] [25] for both supervised and unsupervised flavors of deep learning based homography estimation. For the supervised flavor of the algorithm, we generate synthetic homography warped event frames and train them using the following loss function.

$$\operatorname{argmin}_{\tilde{H}_{4Pt}} \mathbb{E} \left(\left\| \tilde{H}_{4Pt} - \hat{H}_{4Pt} \right\|_2 \right) \quad (6)$$

Here, \tilde{H}_{4Pt} and \hat{H}_{4Pt} are the predicted and ground truth 4-point homographies. We refer the readers to [24] for more details.

For the unsupervised version, we adapt the mathematical formulation [25] for TensorDLT and the Spatial Transformer Network (STN) using bilinear interpolation. The final loss function is given as:

$$\operatorname{argmin}_{\tilde{H}_{4Pt}} \mathbb{E} \left(\mathcal{D} \left(\mathcal{W} \left(\mathcal{E}_t, \tilde{H}_{4Pt} \right), \mathcal{E}_{t+1} \right) \right) \quad (7)$$

where \mathcal{W} is a generic differentiable warp function and can take on different mathematical formulations based on its second argument (model parameters). In this case, \mathcal{W} contains both the TensorDLT and the STN. As before, \mathcal{D} represents a distance measuring image similarity between two event frames (Refer to the supplementary material Section S.II for the mathematical formulations of \mathcal{D}).

D. EVSegFlowNet

The end goal of this work is to detect/segment Independently Moving Objects (IMOs) and to dodge them. One could fragment this problem into two major parts, detecting IMOs, and subsequently estimating their motion to issue a control command to move away from the IMO in a safe manner. Let's start by discussing each fragment. Firstly, we want to segment the object using consecutive event frames \mathcal{E}_t and \mathcal{E}_{t+1} . A simple way to accomplish this is by generating simulated data with known segmentation for each frame and then training a CNN to predict the foreground (IMO)/background segmentation. Such a CNN can be trained using a simple cross-entropy loss function as shown below.

$$\operatorname{argmin}_{p_f} -\mathbb{E} (\mathbb{1}_f \log(p_f) + \mathbb{1}_b \log(p_b)) \quad (8)$$

Here, $\mathbb{1}_f, \mathbb{1}_b$ are the indicator variables denoting if a pixel belongs to foreground or background. They are mutually exclusive, i.e., $\mathbb{1}_f = \neg \mathbb{1}_b$ and p_f, p_b represent the foreground and background predicted probabilities where $p_f + p_b = 1$. Note that each operation in the above equation is performed per pixel, and then an average over all pixels is computed. In the second step we want to estimate the IMO motion. Without any prior knowledge about the IMO it is impossible to estimate the 3D motion of the IMO from a monocular camera (event based or traditional). To make this problem tractable, we assume a prior about the object. More details can be found in Section III.

Once we have a prior about the object, we can estimate the 3D IMO motion using optical flow of the pixels corresponding to the IMO on the image plane. A simple way to obtain optical flow is to train a CNN in a supervised manner. However, recent research has shown that these do not generalize well to new scenes/objects [26]. A better way is to use a self-supervised or completely unsupervised loss function.

$$\operatorname{argmin}_{\hat{\mathbf{x}}} \mathbb{E} (\mathcal{D} (\mathcal{W} (\mathcal{E}_t, \hat{\mathbf{x}}), \mathcal{E}_{t+1})) \quad (9)$$

Here $\hat{\mathbf{x}}$ is the estimated optical flow between $\mathcal{E}_t \mapsto \mathcal{E}_{t+1}$ and \mathcal{W} is a differentiable warp function based on optical flow and bilinear interpolation implemented using an STN. The self-supervised flavor of this algorithm [26] utilizes corresponding image frames instead of event frames for the loss function but the input is still the stack of event frames. One could utilize the two networks we talked about previously and solve the problem of dodging, however, one would need to run two neural networks for this purpose. Furthermore, this method suffers from a major problem: any unsupervised or self-supervised method can estimate rigid optical flow (optical flow corresponding to the background regions \mathcal{B}) accurately but the non-rigid optical flow (optical flow corresponding to the foreground regions \mathcal{F}) is not very accurate. This is an artifact because of the number of pixels corresponding to the foreground is often far less than that corresponding to the background, i.e., $\overline{\mathcal{F}} \ll \overline{\mathcal{B}}$. One would have to train for a lot of iterations to obtain accurate optical flow results on these foreground pixels which runs into the risk of overfitting to the dataset. This defeats the promise of self-supervised or unsupervised formulations.

To solve both the problems of complexity and accuracy, we formulate the problem using a semi-supervised approach to learn segmentation and optical flow at the same time, which we call *EVSegFlowNet*. We call the output of the network *segmentation flow* denoted by $\tilde{\mathbf{p}}$ which is defined as follows.

$$\tilde{\mathbf{p}}_{\mathbf{x}} = \begin{cases} \tilde{\mathbf{p}}_{\mathbf{x}}, & \text{if } \mathbb{1}_f(\mathbf{x}) = 1 \\ \mathbf{0}, & \text{if } \mathbb{1}_b(\mathbf{x}) = 1 \end{cases} \quad (10)$$

One could intuit that we can obtain a noisy segmentation for free by simple thresholding on the magnitude of $\tilde{\mathbf{p}}_{\mathbf{x}}$. To utilize the network to maximum capacity the input to the network is the ego-motion/odometry based warped event frame such that the background pixels in the two input event frames are almost aligned and the only misalignment comes from the IMOs. This ensures that the network's capacity can be utilized fully for learning sub-pixel accurate optical flow for IMO regions. The input to the EVSegFlowNet is $\mathcal{W}(\mathcal{E}_t, \tilde{H}_{4Pt})$ and \mathcal{E}_{t+1} . Here, \tilde{H}_{4Pt} is transformed to E^F before warping.

A complexity analysis of EVSegFlowNet is given in Section S.VI of the supplementary material. The success of our approach can be seen from the experimental results. The loss function for learning $\tilde{\mathbf{p}}_{\mathbf{x}}$ is given below.

$$\operatorname{argmin}_{\tilde{\mathbf{p}}_{\mathbf{x}}} \mathbb{E} \left(\mathcal{D} \left(\mathcal{W} \left(\mathcal{E}'_t, \tilde{\mathbf{p}}_{\mathbf{x}} \right) \circ \mathbb{1}_f, \mathcal{E}_{t+1} \circ \mathbb{1}_f \right) \right) + \lambda_1 \mathbb{E} \left(\left\| \tilde{\mathbf{p}}_{\mathbf{x}} \circ \mathbb{1}_b \right\|_1 \right) + \lambda_2 \mathbb{E} \left(\left\| \tilde{\mathbf{p}}_{\mathbf{x}} \circ \mathbb{1}_b \right\|_2^2 \right) \quad (11)$$

Here, λ_1 and λ_2 are regularization parameters. This loss function is essentially the image difference with elastic net like regularization penalty. This penalty makes the network make background flow zero fairly quickly as compared to simple l_1 or quadratic penalty whilst being robust to outliers (errors in segmentation mask creation).

III. CONTROL POLICY FOR DODGING DYNAMIC OBSTACLES

In this section, we present a solution for evading multiple known and/or unknown IMOs.

Let us consider three different flavors of IMOs: (a) Sphere with known radius r , (b) Unknown shaped objects with

known bound on the size and (c) Unknown objects with no prior knowledge. We tackle each of these cases differently. Knowing the prior information about the geometric nature helps us achieve much more robust results and fine-grain control.

We define \mathcal{F} as the projection of all the IMOs on the image plane such that $\mathcal{F} = \bigcup_{\forall i} \mathcal{F}_i$, where \mathcal{F}_i denotes the i^{th} IMO's image plane projection. Now, let's confabulate each flavor of the problem separately in the following subsections.

A. Sphere with known radius r

Let us first begin with the simplest case, i.e., a *single spherical IMO with known radius r* . On a rectified image the projection of a sphere on the image plane is an ellipse [27]. Evading such an object under no gravitational influence has been tackled and well analyzed by [1]. For spherical objects under the gravitational influence, we estimate the initial 3D position using the known radius information and then we track the object over a few \mathcal{E} to obtain the initial 3D velocity. Here, the tracking is done by detection (segmentation) on every frame.

Assuming a classical physics model, we predict the future trajectory $\mathbf{X}_i^{\text{IMO}}$ of the sphere when it is only under the influence of gravity. Now, we define the point $\mathbf{X}_{i,p}^{\text{IMO}}$ as the intersection of the trajectory $\mathbf{X}_i^{\text{IMO}}$ and the image plane. For the case of a single spherical IMO, we compute the distance between $\mathbf{X}_{i,p}^{\text{IMO}}$ and the initial position of the quadrotor O , denoted by vector $\mathbf{x}_{\min} \in \mathbb{R}^{2 \times 1}$. The "safe" direction is represented as $\mathbf{x}_s = -\mathbf{x}_{\min}$. A simple Proportional-Integral-Derivative (PID) controller based on the differential flatness model of the quadrotor is used with high proportional gain for a quick response to move in the direction \mathbf{x}_s . The minimum amount of movement is equal to the extended obstacle size (the size of the quadrotor is added to the object size).

Now, let's extend to the evasion of *multiple spherical IMOs*. We assume that while objects are detected, there is no occlusion among different IMOs in the front event camera frame. Then, each object \mathcal{F}_i is segmented using mean shift clustering. For each object \mathcal{F}_i , the 3D position and velocity are estimated. It is important to note that since all the objects were targeted at the quadrotor, they are bound to intercept the image plane, say at point $\mathbf{X}_{i,p}^{\text{IMO}}$ (Fig. 4). For evading multiple objects, the quadrotor moves in \mathbf{x}_s direction in the image plane such that $\mathbf{x}_s = (\mathbf{X}_{i,p}^{\text{IMO}} + \mathbf{X}_{i+1,p}^{\text{IMO}})$, where $(\mathbf{X}_{i,p}^{\text{IMO}}, \mathbf{X}_{i+1,p}^{\text{IMO}})$ is a consecutive cyclic pair of vectors for which we solve the following optimization problem:

$$\underset{\mathbf{X}_{i,p}^{\text{IMO}}, \mathbf{X}_{i+1,p}^{\text{IMO}}}{\operatorname{argmin}} \left\langle \frac{\mathbf{X}_{i,p}^{\text{IMO}}}{\|\mathbf{X}_{i,p}^{\text{IMO}}\|_2}, \frac{\mathbf{X}_{i+1,p}^{\text{IMO}}}{\|\mathbf{X}_{i+1,p}^{\text{IMO}}\|_2} \right\rangle \quad (12)$$

where $\langle \cdot, \cdot \rangle$ denotes the inner product/dot product between two vectors. In this case, the size of the biggest IMO is used to execute the control policy as before.

B. Unknown shaped objects with bound on size

Now, consider the case of evading an IMO of an arbitrary shape \mathcal{S} . As the projection of \mathcal{S} on the image plane can be either convex or non-convex, we first obtain the convex hull of \mathcal{S} denoted by \mathcal{H} . Clearly, an evasive maneuver performed using \mathcal{H} guarantees evasion from the object when the rotation of the IMO with respect to the camera is small.

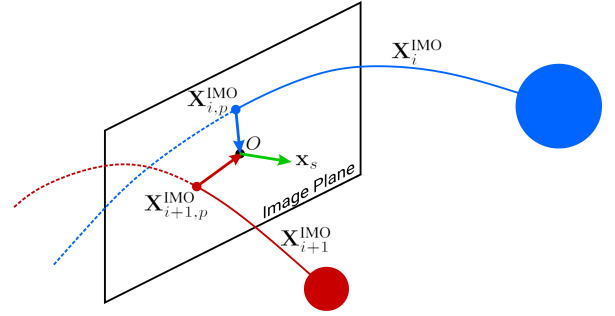


Fig. 4. Vectors $\mathbf{X}_{i,p}^{\text{IMO}}$ and $\mathbf{X}_{i+1,p}^{\text{IMO}}$ represent the intersection of the trajectory and the image plane. \mathbf{x}_s is the direction of the "safe" trajectory. All the vectors are defined with respect to the center of the quadrotor projected on the image plane, O . Both of the spheres are of known radii.

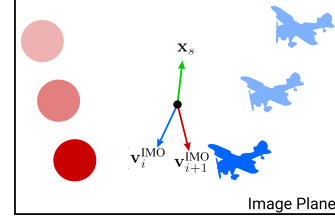


Fig. 5. Representation of velocity direction of multiple unknown IMOs. The vector $\mathbf{v}_i^{\text{IMO}}$ and $\mathbf{v}_{i+1}^{\text{IMO}}$ represent velocities of the corresponding objects. \mathbf{x}_s denotes the "safe" direction for the quadrotor.

Next, we find the principle axes of the projection of \mathcal{H} on the image plane. Because we have a bound on size, i.e., we have a bound on the length of the maximum principle axis in 3D, we can evade this object assuming it to be a sphere of this diameter. Note that this method is more conservative than the previous approach constraining the sensing range and latency based on how close the bound is to actual object size.

C. Unknown objects with no prior knowledge

Without any prior knowledge about the object, it is geometrically infeasible to obtain the 3D velocity of an IMO using a monocular camera. However, we can predict a possible safe trajectory \mathbf{x}_s depending on the velocity direction of the IMOs on the image plane. We compute the unit vector $\mathbf{v}_i^{\text{IMO}}$ in which the IMO is moving by tracking the segmentation mask of the IMO or by computing the mean optical flow direction of the region of interest. For a single unknown IMO, a heuristic is chosen such that the quadrotor moves in the direction perpendicular to the velocity of the IMO on the image plane, i.e., a safe direction for the quadrotor motion which satisfies $\langle \mathbf{x}_s, \mathbf{v}_i^{\text{IMO}} \rangle = 0$.

For evading multiple unknown IMOs, the quadrotor moves in \mathbf{x}_s direction in the image plane such that $\mathbf{x}_s = -(\mathbf{v}_i^{\text{IMO}} + \mathbf{v}_{i+1}^{\text{IMO}})$, where $(\mathbf{v}_i^{\text{IMO}}, \mathbf{v}_{i+1}^{\text{IMO}})$ is a consecutive cyclic pair of unit vectors found by solving the following optimization problem (Fig. 5).

$$\underset{\mathbf{v}_i, \mathbf{v}_{i+1}}{\operatorname{argmin}} \langle \mathbf{v}_i, \mathbf{v}_{i+1} \rangle \quad (13)$$

Note that, we don't have an estimate of how much to move so as to evade the object. Practically, we move as far as possible in the hope of evading the obstacles. Clearly, there is no guarantee of avoiding the IMO in this case and it will depend on the sensing range and latency.



Fig. 6. Objects used in experiments. Left to right: Airplane, car, spherical ball and Bebop 2.

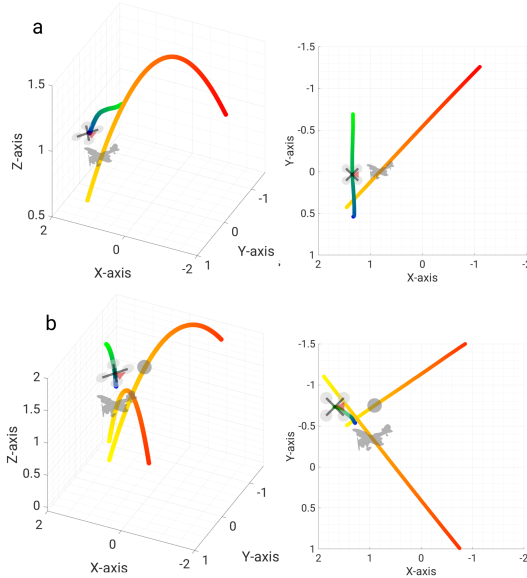


Fig. 7. Vicon estimates for the trajectories of the objects and quadrotor. (a) Perspective and top view for single unknown object case, (b) perspective and top view for multiple object case. Object and quadrotor silhouettes are shown to scale. Time progression is shown from red to yellow for objects and blue to green for the quadrotor.

D. Pursuit: A reversal of evasion?

The generality of our perception stack for navigation is demonstrated by showing that pursuit can be accomplished using a simple reversal of the control policy for the cases presented in III-A and III-B.

Additionally, for an IMO which is self-propelled like a quadrotor, one can perform both pursuit and evade tasks by assuming a linear motion model. Note that here no concept of the agent’s intent is used but it can be introduced with an additional neural network for predicting the motion model of the agent (intent) [28]. We leave this for future work.

In the next section, we provide a detailed experimental analysis and present our results for all the aforementioned cases.

IV. EXPERIMENTS

A. Experimental Setup

A detailed description of the hardware setup is given in Section S.V of the supplementary material.

The experiments were conducted in the Autonomy Robotics and Cognition (ARC) lab’s indoor flying space at the University of Maryland, College Park. The total flying volume is about $6 \times 5.5 \times 3.5 \text{ m}^3$. A Vicon motion capture system with 8 vantage V8 cameras are used to obtain ground truth at 100 Hz. The objects were either thrown or flown (in-case of the bebop experiment) at the quadrotor during hover or slow flight (simulating slow drift) at speeds ranging from 4.4 ms^{-1} to 6.8 ms^{-1} from a distance ranging from 3.6 m to 5.2 m. To enable robust homography estimation, we laid

down carpets of different textures on the ground to obtain strong contours in event frames (Refer to supplementary Fig. S6).

We used four different objects in our experiments, (a) a spherical ball of diameter 140 mm, (b) a car of size $185 \times 95 \times 45 \text{ mm}$ (here a bound of 240 mm is used), (c) an airplane of size $270 \times 250 \times 160 \text{ mm}$ (size information not used in experiments), (d) a Bebop 2 of size $330 \times 380 \times 200 \text{ mm}$. Also, we used an integration time δt of 30 ms for all our experiments.

B. Experimental Results and Discussion

In this paper, we considered the case of navigating through different sets of multiple dynamic obstacles. We dealt with six different evading combinations and one pursuit experiment: (a) Spherical ball with a known radius of 140 mm, (b) car with a bound on the maximum dimension size of 240 mm, (c) airplane with no prior information, (d) Bebop 2 flying at a constant velocity, (e) multiple unknown objects, (f) pursuit of Bebop 2 and (g) low-light dodging experiment. For each evasion case, the objects are directly thrown towards the Aero quadrotor such that a collision would definitely occur if the Aero holds its initial position. The objects used in the experiments are shown in Fig. 6. For each case, a total of 30 trials were conducted. The Vicon plots for cases (c) and (e) are shown in Fig. 7. Notice that the objects would have hit the quadrotor if it had not moved from its initial position. We achieved a remarkable success rate of 86% in cases (a) and (b), 76% in case (c). Both Parrot Bebop 2 experiments (case (d), (f)) resulted in 83% success rate. Case (e) was carefully performed with synchronized throws between the two objects and resulted about 76% success rate. For the low-light experiment (case (g)), we achieved a success rate of 70%. Here success is defined as both a successful detection and evasion for the evade experiments and both a successful detection and collision for the pursuit task. Fig. 8 shows sequences of images for cases (a)-(f) along with sample front facing event frame and segmentation outputs.

Before the IMO is thrown at the quadrotor, the quadrotor maintains its position (hover) using the differential X^W and Y^W estimates from the EVHomographyNet and Z^W estimates from the sonar.

When the IMO is thrown at the quadrotor, the IMO is detected for five consecutive frames to estimate either the trajectory or image plane velocity and to remove outliers using simple morphological operations. This gives a perception response lag of 60 ms (each consecutive frame pair takes 10 ms for the neural network computation and 2 ms for the post-processing). Finally, the quadrotor moves using the simple PID controller presented before.

Note that, we talked about obtaining both segmentation and optical flow from EVSegFlowNet. This was based on the conceptualization of optical flow being used for other tasks as well. However, if only the dodging task is to be performed, a smaller segmentation network can be used without much loss of accuracy.

Fig. 9 shows the input and output of EVDeBlurNet for losses \mathcal{D}_2 and \mathcal{D}_3 under $\delta t = \{1, 5, 10\} \text{ ms}$. Observe the amount of noise (stray events not associated with strong contours) in the raw images (top row of Fig. 9). The second row shows the output of EVDeBlurNet for \mathcal{D}_2 loss. Observe that this works well for smaller integration times but for larger integration times, the amount of denoising and deblurring performance deteriorates. However, \mathcal{D}_3 loss

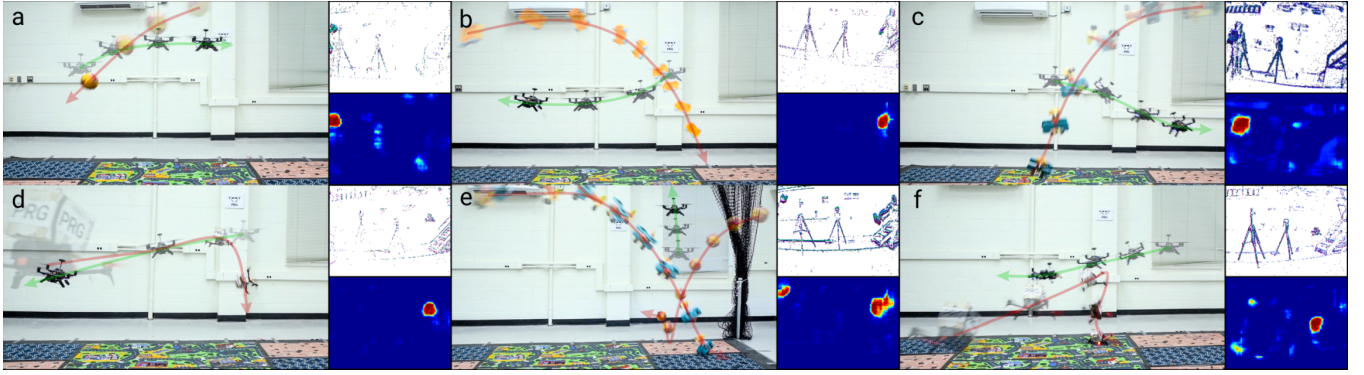


Fig. 8. Sequence of images of quadrotor dodging or persuading of objects. (a)-(d): Dodging a spherical ball, car, airplane and Bebop 2 respectively. (e): Dodging multiple objects simultaneously. (f): Pursuit of Bebop 2 by reversing control policy. Object and quadrotor transparency show progression of time. Red and green arrows indicate object and quadrotor directions respectively. On-set images show front facing event frame (top) and respective segmentation obtained from our network (down).

TABLE I
QUANTITATIVE EVALUATION OF DIFFERENT METHODS FOR HOMOGRAPHY ESTIMATION.

Method (Loss)	RMSE _i in px.					RMSE _o in px.				
	$\gamma = \pm[0, 5]$	$\gamma = \pm[6, 10]$	$\gamma = \pm[11, 15]$	$\gamma = \pm[16, 20]$	$\gamma = \pm[21, 25]$	$\gamma = \pm[0, 5]$	$\gamma = \pm[6, 10]$	$\gamma = \pm[11, 15]$	$\gamma = \pm[16, 20]$	$\gamma = \pm[21, 25]$
Identity	3.92 \pm 0.83	11.40 \pm 0.70	18.43 \pm 0.70	25.50 \pm 0.70	32.55 \pm 0.71	3.92 \pm 0.84	11.40 \pm 0.70	18.44 \pm 0.71	25.49 \pm 0.70	32.55 \pm 0.71
S	3.23 \pm 1.13	3.90 \pm 1.34	5.31 \pm 2.05	9.63 \pm 4.57	17.65 \pm 7.00	4.15 \pm 1.78	5.05 \pm 2.19	6.99 \pm 3.11	11.21 \pm 4.84	18.37 \pm 6.61
US* (\mathcal{D}_1)	2.97 \pm 1.22	3.84 \pm 1.61	5.99 \pm 2.78	11.64 \pm 5.69	20.36 \pm 7.68	3.92 \pm 1.53	5.31 \pm 2.43	8.14 \pm 3.86	13.63 \pm 5.87	21.22 \pm 7.35
US* (\mathcal{D}_2)	2.48 \pm 0.93	3.53 \pm 1.43	5.89 \pm 2.70	11.74 \pm 5.69	20.51 \pm 0.70	3.19 \pm 1.26	4.86 \pm 2.31	7.92 \pm 3.73	13.47 \pm 5.71	21.22 \pm 7.08
DB + S	2.73 \pm 1.01	3.16 \pm 1.23	4.00 \pm 1.79	6.50 \pm 3.54	12.22 \pm 6.58	3.69 \pm 1.51	4.49 \pm 2.10	5.91 \pm 3.16	9.04 \pm 4.90	14.60 \pm 6.95
DB + US (\mathcal{D}_1)	2.19 \pm 0.88	3.04 \pm 1.57	4.99 \pm 2.75	10.16 \pm 5.54	18.62 \pm 7.85	3.08 \pm 1.37	4.63 \pm 2.68	7.57 \pm 4.30	13.16 \pm 6.25	21.08 \pm 7.49
DB + US (\mathcal{D}_2)	2.41 \pm 1.06	3.30 \pm 1.77	5.36 \pm 3.02	10.39 \pm 5.78	18.77 \pm 8.07	3.35 \pm 1.76	5.05 \pm 3.03	8.11 \pm 4.65	13.46 \pm 6.48	21.08 \pm 7.81

* Trained for 100 epochs on supervised and then fine-tuned on unsupervised for 100 more epochs. γ denotes the perturbation range in px. for evaluation.

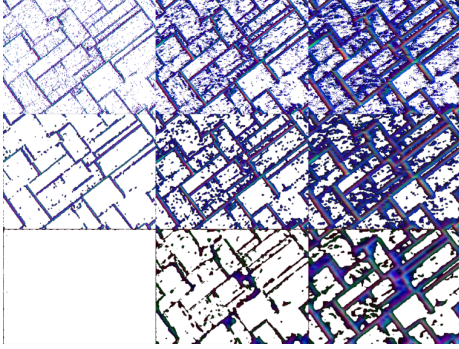


Fig. 9. Output of EVDeBlurNet for different integration time and loss functions. Top row: raw event frames, middle row: deblurred event frames with \mathcal{D}_2 and bottom row: deblurred event frames with \mathcal{D}_3 with δt . Left to right: δt of 1 ms, 5 ms and 10 ms. Notice that only the major contours are preserved and blurred contours and thinned in deblurred outputs.

which is aimed at outlier rejection is more suppressive of weak contours and hence one can observe that the frame has almost no output for smaller integration times. This has the effect of working well for larger integration times.

Fig. 10 shows the output of EVHomographyNet using the supervised loss function on both raw (top row) and deblurred frames (bottom row). Observe that the deblurred homography estimation is more robust to changes in different integration times. Table I shows the quantitative evaluation of different methods used for training EVHomographyNet. Here, RMSE_i and RMSE_o denote the average root mean square error [25] in the testing dataset with textures similar to that of the training set, and completely novel textures respectively. RMSE_o quantifies how well the network can generalize to unseen samples. Notice that the supervised flavors of the algorithm work better (lower RMSE_i and RMSE_o) than their respective unsupervised counterparts. We speculate that

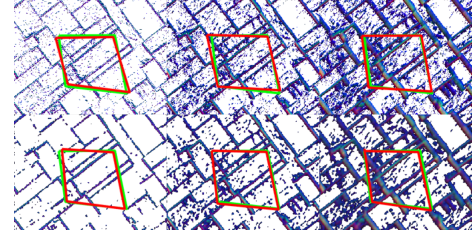


Fig. 10. Output of EVHomographyNet for raw and deblurred event frames at different integration times. Green and red color denotes ground truth and predicted H_{APt} respectively. Top row: raw events frames and bottom row: deblurred event frames. Left to right: δt of 1 ms, 5 ms and 10 ms. Notice that the deblurred homography outputs are almost not affected by integration time.

this is because of the sparsity in data and that the simple image based similarity metrics not being well suited for event frames. We leave crafting a novel loss function for event frames as a potential avenue for future work. Also, notice how deblur variants of the algorithms almost always work better than their respective non-deblurred counterparts highlighting the utility of EVDeblurNet.

TABLE II
QUANTITATIVE EVALUATION OF DIFFERENT METHODS FOR SEGMENTATION OF IMO.

Method (Loss)	DR _i in %	DR _o in %	Run Time in ms	FLOPs in M	Num. Params in M
SegNet	40.4	49.0	1.5	222	0.03
DB + SegNet	68.7	81.5	7.5	4900	2.33
DB + H + SegNet	69.1	83.2	10	5150	3.63
SegFlowNet	81.9	88.3	1.5	222	0.03
DB + SegFlowNet	90.1	93.3	7.5	4900	2.33
DB + H + SegFlowNet	90.7	93.4	10	5150	3.63

Table II shows the quantitative results of different variants of segmentation networks trained using the \mathcal{D}_2 loss for SegFlowNet. Here DB denotes the deblurred outputs produced using the combination of \mathcal{D}_2 and \mathcal{C}_2 loss. Also, H

denotes the stack of warped \mathcal{E}_t and \mathcal{E}_{t+1} using the outputs of the network DB + S in Table I. Here DR denotes the detection rate and is defined as:

$$DR = \mathbb{E} \left(\frac{(\overline{(\mathcal{D} \cap \mathcal{G}) \circ \mathbb{1}_{\mathcal{E}}})}{(\overline{\mathcal{G} \circ \mathbb{1}_{\mathcal{E}}})} \geq \tau \right) \times 100\% \quad (14)$$

where \mathcal{G} and \mathcal{D} denote the ground truth and predicted masks respectively, and $\mathbb{1}_{\mathcal{E}}$ denotes the presence of an event in either of the input event frames. For our evaluation, we choose $\tau = 0.5$. Notice that using both deblur and homography warping helps improve the results as anticipated. Again, DR_i and DR_o denote testing on trained objects and completely novel objects. As before, deblurring helps generalize much better to novel objects and deblurring with homography warping gives better results showing that the network's learning capacity is utilized better.

The network architectures and training details are provided in the Section S.III of the supplementary material.

V. CONCLUSIONS

We presented an AI-based algorithmic design for micro/nano quadrotors, taking into account the knowledge of the system's computation and latency requirements using deep learning. The central conception of our approach is to contrive AI building blocks using shallow neural networks which can be re-purposed. This philosophy was used to develop a method to dodge dynamic obstacles using only a monocular event camera and on-board sensing. To our knowledge, this is the first deep learning based solution to the problem of dynamic obstacle avoidance using event cameras on a quadrotor. Moreover, our networks are trained in simulation and directly transfer to the real world without fine-tuning or retraining. We also show the generalizability of our navigation stack by extending our work to the pursuit task. As a parting thought, a better similarity scoring metric between event frames or a more robust construction of event frames can improve our results.

ACKNOWLEDGEMENT

This work was partly funded by the Brin Family Foundation, National Science Foundation under grant BCS 1824198, ONR under grant N00014-17-1-2622, the Northrop Grumman Mission Systems University Research Program. The authors would like to thank NVIDIA for the grant of an NVIDIA Titan-Xp GPU and Intel for the grant of the Intel Aero Platform.

REFERENCES

- [1] D. Falanga, S. Kim, and D. Scaramuzza. How Fast Is Too Fast? The Role of Perception Latency in High-Speed Sense and Avoid. *IEEE Robotics and Automation Letters*, 4(2):1884–1891, April 2019.
- [2] Pierre Sermanet, Raia Hadsell, Jan Ben, Ayse Naz Erkan, Beat Flepp, Urs Muller, and Yann LeCun. Speed-range dilemmas for vision-based navigation in unstructured terrain. *IFAC Proceedings Volumes*, 40(15):300–305, 2007.
- [3] Guillermo Gallego, Tobi Delbruck, Garrick Orchard, Chiara Bartolozzi, Brian Taba, Andrea Censi, Stefan Leutenegger, Andrew Davison, Joerg Conradt, Kostas Daniilidis, et al. Event-based vision: A survey. *arXiv preprint arXiv:1904.08405*, 2019.
- [4] Antoni Rosinol Vidal, Henri Rebecq, Timo Horstschaefer, and Davide Scaramuzza. Ultimate SLAM? Combining events, images, and IMU for robust visual SLAM in HDR and high-speed scenarios. *IEEE Robotics and Automation Letters*, 3(2):994–1001, 2018.
- [5] Michael Bloesch, Sammy Omari, Marco Hutter, and Roland Siegwart. Robust visual inertial odometry using a direct ekf-based approach. In *2015 IEEE/RSJ international conference on intelligent robots and systems (IROS)*, pages 298–304. IEEE, 2015.
- [6] C. Forster, L. Carlone, F. Dellaert, and D. Scaramuzza. On-Manifold Preintegration for Real-Time Visual-Inertial Odometry. *IEEE Transactions on Robotics*, 33(1):1–21, 2017.
- [7] Tong Qin, Peiliang Li, and Shaojie Shen. VINS-Mono: A robust and versatile monocular visual-inertial state estimator. *IEEE Transactions on Robotics*, 34(4):1004–1020, 2018.
- [8] Alex Zihao Zhu, Nikolay Atanasov, and Kostas Daniilidis. Event-based visual inertial odometry. In *2017 IEEE Conference on Computer Vision and Pattern Recognition (CVPR)*, pages 5816–5824. IEEE, 2017.
- [9] Huai-Jen Liang, Nitin J Sanket, Cornelia Fermüller, and Yiannis Aloimonos. SalientDSO: Bringing attention to direct sparse odometry. *IEEE Transactions on Automation Science and Engineering*, 2019.
- [10] Sean L Bowman, Nikolay Atanasov, Kostas Daniilidis, and George J Pappas. Probabilistic data association for semantic SLAM. In *2017 IEEE International Conference on Robotics and Automation (ICRA)*, pages 1722–1729. IEEE, 2017.
- [11] R. Sabzevari and D. Scaramuzza. Multi-body motion estimation from monocular vehicle-mounted cameras. *IEEE Transactions on Robotics*, 2016.
- [12] Valentina Vasco, Arren Glover, Elias Mueggler, Davide Scaramuzza, Lorenzo Natale, and Chiara Bartolozzi. Independent motion detection with event-driven cameras. In *2017 18th International Conference on Advanced Robotics (ICAR)*, pages 530–536. IEEE, 2017.
- [13] Anton Mitrokhin, Cornelia Fermüller, Chethan Parameshwara, and Yiannis Aloimonos. Event-based moving object detection and tracking. In *2018 IEEE/RSJ International Conference on Intelligent Robots and Systems (IROS)*, pages 1–9, Oct 2018.
- [14] Timo Stoffregen, Guillermo Gallego, Tom Drummond, Lindsay Kleeman, and Davide Scaramuzza. Event-based motion segmentation by motion compensation. In *International Conference on Computer Vision (ICCV)*, 2019.
- [15] Anton Mitrokhin, Chengxi Ye, Cornelia Fermüller, Yiannis Aloimonos, and Tobi Delbruck. Ev-imo: Motion segmentation dataset and learning pipeline for event cameras. *arXiv preprint arXiv:1903.07520*, 2019.
- [16] H Alvarez, Lina María Paz, Jürgen Sturm, and Daniel Cremers. Collision avoidance for quadrotors with a monocular camera. In *Experimental Robotics*, pages 195–209. Springer, 2016.
- [17] Nitin J Sanket, Chahat Deep Singh, Kanishka Ganguly, Cornelia Fermüller, and Yiannis Aloimonos. GapFlyt: Active vision based minimalist structure-less gap detection for quadrotor flight. *IEEE Robotics and Automation Letters*, 3(4):2799–2806, Oct 2018.
- [18] Andrew J Barry, Peter R Florence, and Russ Tedrake. High-speed autonomous obstacle avoidance with pushbroom stereo. *Journal of Field Robotics*, 35(1):52–68, 2018.
- [19] Kartik Mohta, Michael Watterson, Yash Mulgaonkar, Sikang Liu, Chao Qu, Anurag Makineni, Kelsey Saulnier, Ke Sun, Alex Zhu, Jeffrey Delmerico, et al. Fast, autonomous flight in gps-denied and cluttered environments. *Journal of Field Robotics*, 35(1):101–120, 2018.
- [20] Kartik Mohta, Ke Sun, Sikang Liu, Michael Watterson, Bernd Pfrommer, James Svacha, Yash Mulgaonkar, Camillo Jose Taylor, and Vijay Kumar. Experiments in fast, autonomous, gps-denied quadrotor flight. In *2018 IEEE International Conference on Robotics and Automation (ICRA)*, pages 7832–7839. IEEE, 2018.
- [21] Elias Mueggler, Nathan Baumli, Flavio Fontana, and Davide Scaramuzza. Towards evasive maneuvers with quadrotors using dynamic vision sensors. In *2015 European Conference on Mobile Robots (ECMR)*, pages 1–8. IEEE, 2015.
- [22] Guillermo Gallego, Henri Rebecq, and Davide Scaramuzza. A unifying contrast maximization framework for event cameras, with applications to motion, depth, and optical flow estimation. In *The IEEE Conference on Computer Vision and Pattern Recognition (CVPR)*, June 2018.
- [23] Guillermo Gallego, Christian Forster, Elias Mueggler, and Davide Scaramuzza. Event-based camera pose tracking using a generative event model. *arXiv preprint arXiv:1510.01972*, 2015.
- [24] Daniel DeTone, Tomasz Malisiewicz, and Andrew Rabinovich. Method and system for performing convolutional image transformation estimation, November 23 2017. US Patent App. 15/600,545.
- [25] Ty Nguyen, Steven W Chen, Shreyas S Shivakumar, Camillo Jose Taylor, and Vijay Kumar. Unsupervised deep homography: A fast and robust homography estimation model. *IEEE Robotics and Automation Letters*, 3(3):2346–2353, 2018.
- [26] Alex Zihao Zhu, Liangzhe Yuan, Kenneth Chaney, and Kostas Daniilidis. Ev-flownet: self-supervised optical flow estimation for event-based cameras. *arXiv preprint arXiv:1802.06898*, 2018.
- [27] Clarence Raymond Wylie. *Introduction to projective geometry*. Courier Corporation, 2011.
- [28] Riccardo Spica, Davide Falanga, Eric Cristofalo, Eduardo Montijano, Davide Scaramuzza, and Mac Schwager. A real-time game theoretic planner for autonomous two-player drone racing. *arXiv preprint arXiv:1801.02302*, 2018.